

Thermal Performance Enhancement of Adaptive Optics by Use of a Deformable Secondary Mirror

MICHAEL LLOYD-HART

Center for Astronomical Adaptive Optics, University of Arizona, Tucson, AZ 85721; mhart@as.arizona.edu

Received 1999 May 26; accepted 1999 October 7

ABSTRACT. An adaptive optics system is being built for the 6.5 m Multiple Mirror Telescope (MMT) conversion on Mount Hopkins for diffraction-limited observations in the near-infrared. At the heart of the system is a deformable secondary mirror which introduces corrections to the optical wavefront. By compensating these errors at the telescope's secondary, the system has been optimized for low thermal emissivity and high photon throughput. The scientific productivity of the facility will thereby be enhanced in comparison with a telescope equipped with more conventional adaptive optics. The Large Binocular Telescope under construction on Mount Graham will also use adaptive secondary mirrors. This paper explores the benefit to both facilities in terms of the integration time required to achieve a given signal-to-noise ratio. The gain is found to be substantial in the photometric bands *K*, *L*, *M*, and *N*.

1. BACKGROUND

The old six-mirror Multiple Mirror Telescope (MMT) has been dismantled to make way for its conversion to a single 6.5 m telescope (West et al. 1996). Engineering first light with the new telescope occurred at prime focus in 1999 October. Shortly thereafter, measurements with a Shack-Hartmann wavefront sensor began, also at prime focus, which confirm the excellent quality of the site. The first rigid secondary mirror, in an *f*/9 Cassegrain configuration, is expected by 2000 January.

In parallel with construction of the telescope, a sophisticated adaptive optics (AO) system is being built with the aim of providing imaging and spectroscopy at the diffraction limit of resolution in the near-infrared, from 1.5 to 10 μm (Lloyd-Hart et al. 1998). One of the key innovations is the use of a deformable secondary mirror as the wavefront correcting element (Salinari & Sandler 1998). Many technical challenges have been successfully met in the development of the secondary; the motivation for tackling them has been the strong desire to overcome the problems of thermal emissivity and throughput presented by more traditional AO systems.

The MMT will be the first telescope to be equipped with an adaptive secondary. Following shortly after will be the twin 8.4 m telescopes of the Large Binocular Telescope (LBT) (Gray, West, & Gallieni 1996). Currently under construction on Mount Graham in southeast Arizona, both units of the telescope will be fitted with adaptive secondaries in the Gregorian configuration. No other secondary mirrors are presently planned.

The standard approach to AO, exemplified by systems at the W. M. Keck Telescope (Wizinowich et al. 1998) and the US Air Force's Starfire Optical Range (Fugate et al. 1991), employs optics downstream of the telescope to image the entrance pupil on a separate deformable mirror, and then further optics to bring the light to the focal plane of a science detector. Since it has not yet proved practical to put all these optics in a cryogenic environment, the impact of the additional warm surfaces on observations in the thermal infrared is significant.

By compensating optical aberrations at the secondary mirror which must in any case be part of the telescope, the corrected beam may be brought straight into the science dewar. This has been the approach in the design of the MMT AO system, in which the entrance window to the dewar is a dichroic beam splitter that transmits infrared and reflects visible light into a wavefront sensor.

The scientific benefit of an adaptive secondary is perhaps best stated in terms of the integration time required to make an observation of given signal-to-noise ratio (S/N) on a given source. A theoretical comparison is made below between two systems on a 6.5 m telescope, correcting to the diffraction limit, one of which uses an adaptive secondary, while the other relies on corrections at a reimaged pupil. In each case, the optically simpler design has a clear advantage, particularly in the atmospheric windows represented by the photometric bands *K*, *L*, *M*, and *N*.

Comparisons are also drawn with systems in use or under construction at a number of other telescopes in the 8–10 m class. Relative times have been derived for each of these

telescopes to reach a background-limited source compared to both the MMT and the LBT. It is found that in the same four bands even the smaller 6.5 m telescope, using an adaptive secondary, outperforms its larger brethren using standard AO systems.

2. DESCRIPTION OF THE MODELED SYSTEMS

The two systems being compared on 6.5 m telescopes are shown schematically in Figure 1. The assumed characteristics of the optics are summarized in Table 1, the important quantities being the overall transmission and emissivity of the optics in front of the dewar, which are assumed to be independent of wavelength. These quantities are used in the next section to derive expressions for the observed flux at the detector.

Rather conservative values have been adopted for the reflectivity of the mirrored surfaces in both systems. Although better values can certainly be obtained in the laboratory environment, the situation at the telescope is far less forgiving. Dust, insect parts, and metal oxide all accumulate on the surface of the primary mirror between metalizings and lead to a gradual degradation of the reflectivity, with a corresponding increase in thermal emissivity. Data from the 3.5 m WIYN telescope on Kitt Peak show that even given monthly cleanings with CO₂, reflectivity typically drops by 3% after 6 months (J. R. Hutchinson 1999, private communication). Because the secondary mirror in its downward-looking orientation generally accumulates less dust than the primary, its reflectivity is assumed to be somewhat higher.

Additional relay optics are required in the unoptimized AO system. These have been modeled as five reflective sur-

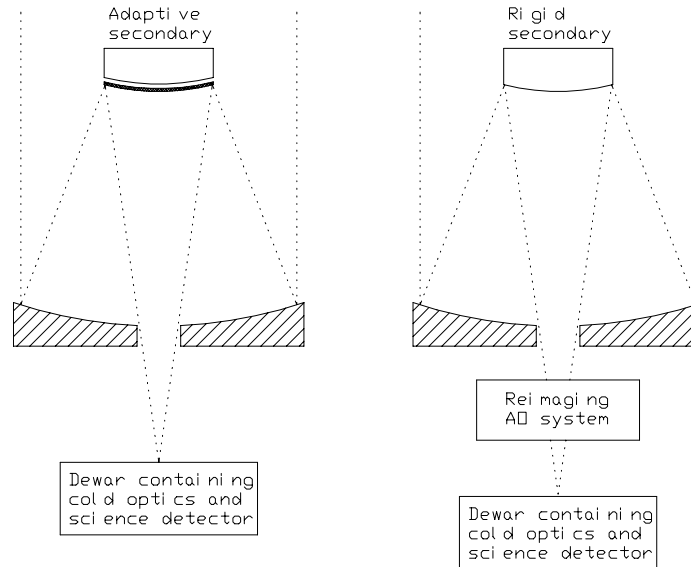


FIG. 1.—Schematic view of the two optical systems compared in this paper. In each case, a telescope with a 6.5 m primary mirror uses adaptive optics to correct wavefront aberration before bringing the light to an infrared science detector via cold optics in a dewar. In the thermally optimized case (left), corrections are introduced at a deformable secondary mirror, while in the other case (right), reimaging optics are used to map an image of the primary onto a separate deformable mirror.

TABLE 1
MODEL PARAMETERS

Parameter	Optimized	Unoptimized
Primary mirror diameter (D)	6.5 m	6.5 m
Primary mirror reflectivity (R_p)	0.95	0.95
Secondary mirror reflectivity (R_s)	0.97	0.97
Reflectivity of additional surfaces (R_a)	...	0.98
Transmissivity of additional surfaces (T_a)	...	0.98
Number of additional reflective surfaces (m)	0	5
Number of additional transmissive surfaces (n)	0	2
Total throughput of system ($\eta = R_p R_s R_a^m T_a^n$)	0.92	0.80
System emissivity (ϵ)	0.079	0.200

faces and one transmissive element (two surfaces). The optical efficiency of these extra elements is assumed to be rather good, though not perfect, since they will typically be in a much better controlled environment than the telescope itself. This optical train approximates the PUEO system which mounts at the Cassegrain focus of the Canada-France-Hawaii Telescope (Rigaut et al. 1998). PUEO implements perhaps the best practical design from the point of view of thermal performance without relying on an adaptive secondary. Between the telescope and the infrared science camera are a fold flat, a collimator mirror, the deformable mirror, a reimaging mirror which doubles as a fast tilt mirror, and a second fold flat. In addition, the science light path includes a dichroic beam splitter to separate the infrared beam from the visible light used for wavefront sensing and an optional atmospheric dispersion corrector (ADC).

The MMT system also includes an ADC, but it is inside the dewar, and so makes no contribution to the thermal background over the wavelength range of interest. Since it is in principle possible to put the ADC of any AO system in the cold environment, the PUEO design as modeled here is modified in this way, to match the design of the adaptive secondary system.

Strictly enforcing the minimization of warm optics means that the correction of global image motion, accomplished by a separate tip-tilt mirror in PUEO, as in most AO systems, must be done at the secondary mirror along with the higher order corrections. The response time of such a massive piece of glass to large-scale motion commands is then of concern. In fact, the bandwidth of the adaptive secondary for the MMT is better than that of most small fast-steering mirrors. This is because all the actuators are used to drive the tip and tilt modes, so each actuator must overcome the inertia of only its small portion of the mirror, which weighs about 10 g.

The two AO systems are assumed to provide the same degree of wavefront correction. Under median conditions at the MMT site, the AO system now under construction, which can control up to 216 degrees of freedom, is expected to correct the image to a Strehl ratio of 0.5 in the K band (Sandler et al. 1994) on the basis of a laser beacon. At longer wavelengths, correspondingly higher Strehl ratios will be seen. In the N band, the diffraction limit can be reached with just tip-tilt control. No higher order compensation is required, although some scientific programs such as the investigation of circumstellar environments at around $10\ \mu\text{m}$ using nulling interferometry (Hinz et al. 1998) can be greatly enhanced by correcting the image to very high Strehl ratio in order to reduce photon noise from the star. Results presented in § 5 have therefore been computed over the range $2\text{--}15\ \mu\text{m}$ of thermal infrared wavelengths for which some level of AO compensation is valuable.

Only photon noise is considered in the computation of the S/N. In particular, detector read noise and dark current

are neglected. Detectors with rms read noise less than $10\ e^-$ already exist in the $1\text{--}5\ \mu\text{m}$ range, and they are expected to improve further. Since the dark current for these detectors of less than $1\ e^- \text{ pixel}^{-1} \text{ s}^{-1}$ is in almost all cases lower than the sky background flux, it is generally possible to take exposures that are background or source limited rather than detector limited. The one exception is shortward of $2.3\ \mu\text{m}$, where the sky background is dominated by a forest of OH emission lines, with very dark regions in between. In the case of high-resolution spectroscopy at these wavelengths, when the lines are resolved, there may be parts of the spectrum dominated by detector effects. In the $5\text{--}15\ \mu\text{m}$ region, the state of the art is still advancing, but detectors are already at the point where they are not at all limited by read noise or dark current even when used for spectroscopy.

3. SOURCES OF PHOTON NOISE

To compute the relative time required by the two systems to make an observation of given S/N, all significant sources of flux detected at the science camera must be identified. The final detected photon flux F may be written as the sum of five terms:

$$F = F_{\text{thermal}} + F_{\text{sky}} + F_{\text{scatter}} + F_{\text{target}} + F_{\text{stray}}. \quad (1)$$

These terms arise, respectively, from thermal radiation from warm optics in the beam and obscurations such as the secondary spider, thermal and OH emission from the sky, light from all sources scattered into the beam by dust and surface roughness of the optics, flux from the science target itself, and stray ambient light from leaks in the optical system. They are considered individually below, with the exception of F_{stray} . This is not a fundamental source of radiation and can with care be reduced to an arbitrarily low level. It is ignored in the subsequent discussion.

Note that the expressions given below for the contributions to F do not allow for the throughput of the cold optics or the quantum efficiency of the science detector. These are assumed to be the same in both cases and therefore cancel out in the final expression for the ratio of integration times. In addition, no account is taken of the zenith angle of the observation. The MMT AO system will rely on a sodium laser guide beacon as its primary source of wavefront information. Since use of the laser is restricted to zenith angles less than 45° , the effect of observing off the zenith will not be large.

3.1. Thermal Radiation from the Optics

Thermal radiation from warm surfaces in the science beam is by far the most significant term in equation (1) from the point of view of the present analysis, since it is the

reduction of F_{thermal} in the adaptive secondary system which is its main advantage. Under the assumption that the radiating surfaces look strictly like blackbodies, the flux F_{thermal} seen by a pixel of angular extent p projected onto the sky is given by

$$F_{\text{thermal}} = \epsilon A p^2 P_{\lambda} . \quad (2)$$

In this equation, ϵ is the effective combined emissivity of all surfaces in front of the science dewar, including the effects of steps taken to prevent emission from reaching the detector, such as Lyot stops; A is the area of the telescope aperture; and P_{λ} is the Planck function for the photon flux in the wavelength range λ_1 to λ_2 :

$$P_{\lambda} = 2 \int_{\lambda_1}^{\lambda_2} \frac{c}{\lambda^4} \frac{1}{e^{hc/\lambda kT} - 1} d\lambda . \quad (3)$$

The thermal flux is of course strongly dependent on the temperature of the radiating surfaces. In this analysis, the temperature T is taken to be that of ambient air. Figure 2 shows a histogram of temperatures measured in the MMT chamber with the building shutters open, just before dawn (Milone, Heller, & McAfee 1999). The mean value is 8.2°C. The figure summarizes 363 measurements taken roughly uniformly through the 2 years 1996 and 1997. Temperatures were recorded only on nights when observing actually took place, so the data are representative of conditions that will be experienced by the AO system in use.

3.2. Sky Background

Background radiation from molecules in the atmosphere, particularly water and OH, becomes very significant as one moves into the thermal infrared. The flux observed by a single pixel is

$$F_{\text{sky}} = \eta A p^2 S_{\lambda} , \quad (4)$$

where η is the overall throughput of the optics. To quantify F_{sky} , S_{λ} has been computed from a model of the background radiation above Mauna Kea. Although not specific to the atmosphere above Mount Hopkins, the model, shown in Figure 3a, is by far the most comprehensive available in the wavelength region of interest. Site-to-site variation in atmospheric background is largely due to water vapor. Studies above Mount Lemmon, approximately 80 km north of Mount Hopkins (Warner 1977), have shown that except during the summer monsoon season, the region is comparably dry to Mauna Kea, with 1–3 mm precipitable water vapor.

Figure 3b shows the atmospheric transmission over the same wavelength region, also for Mauna Kea. There are five

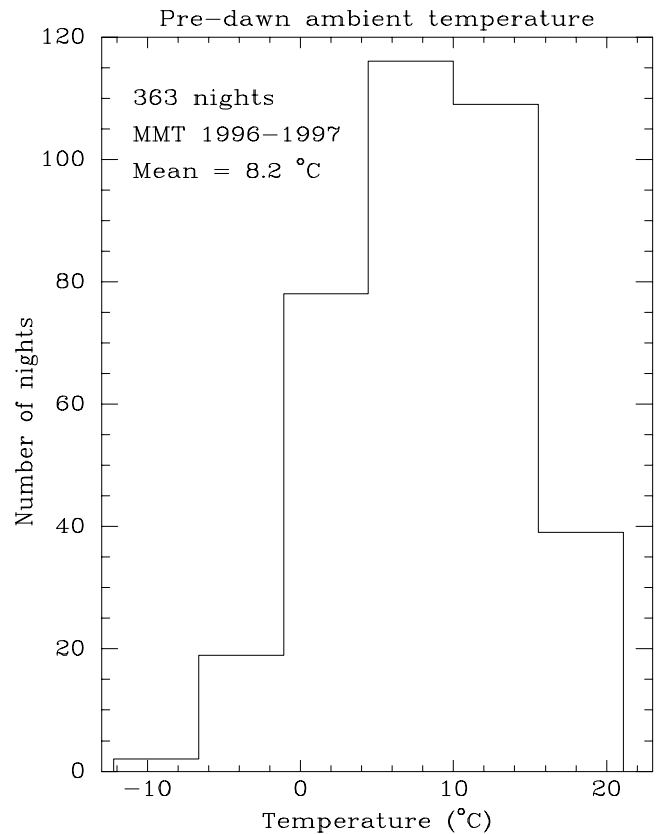


FIG. 2.—Observed ambient temperature distribution inside the MMT chamber with the building shutters open, recorded on 363 nights just before dawn. The sampling is roughly uniform throughout 1996 and 1997 and represents only those nights during which observing actually took place.

distinct windows of low opacity which correspond to the photometric bands H through N . Observing outside these windows is extremely difficult from the ground; the results presented in § 5 account only for wavelength regions where the atmospheric transmission is greater than 20%.

3.3. Scattered Light

Dust on the optical surfaces and microroughness of the polished glass lead to scattering of thermal and sky background radiation into the beam. A simple analysis however shows that the effect is negligible for optics of high quality. Consider first that thermal radiation from the telescope and its environment, and background light from the sky, will be scattered into the observed beam from at most 2π steradians per optical surface. For good optics coated with a small amount of dust, the bidirectional scattering distribution function has a value of $\beta = 2 \times 10^{-15}/\lambda^2 \text{ sr}^{-1}$, where the wavelength λ is in meters (Bawolek et al. 1993). The photon flux scattered into the field of view of a single pixel is

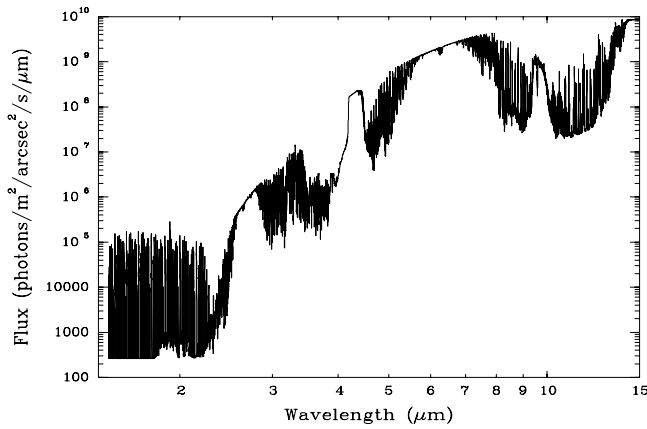


FIG. 3a

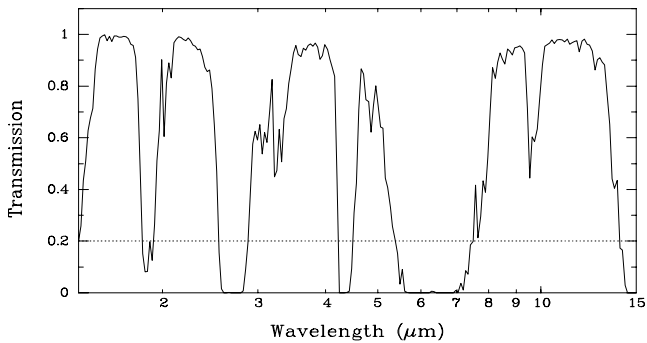


FIG. 3b

FIG. 3.—Assumed model of the atmosphere, derived from measurements taken at Mauna Kea. (a) Background radiation, primarily from OH and water vapor; (b) atmospheric transmission.

then at most

$$F_{\text{scatter}} = 2\pi A(NP_{\lambda} + \eta S_{\lambda})\beta p^2. \quad (5)$$

In this equation, it is assumed that thermal background flux of $2\pi AP_{\lambda}$ is incident on each of N surfaces, and radiation from the sky is incident on one surface, namely, the primary mirror. Of the incident radiation, a fraction βp^2 is scattered into the field of view of each pixel.

By comparing this expression to equations (2) and (4) above for the thermal and sky radiation, it can be shown that scattering is negligible provided that

$$\frac{P_{\lambda}}{S_{\lambda}} \gg \frac{(2\pi\beta - 1)\eta}{\epsilon - 2\pi\beta N}, \quad (6)$$

since in that case $F_{\text{scatter}} \ll F_{\text{thermal}} + F_{\text{sky}}$. With the values adopted for the model, this inequality is satisfied by at least an order of magnitude at all wavelengths of concern, and so in the present work, scattering is not considered further. It should be noted that ignoring F_{scatter} provides a conservative comparison between the two AO systems, since the

unoptimized system suffers from more noise due to thermal background scattering because of its higher count of potentially scattering optical surfaces.

3.4. Light from the Target Source

If the photon flux from an extended source in the sky is B (in units of photons $\text{m}^{-2} \text{arcsec}^{-2} \text{s}^{-1}$), then the detected flux per pixel is

$$F_{\text{target}} = \eta A p^2 B. \quad (7)$$

If the source is not resolved, then one must be more careful about the angular dependence. In the following analysis, the plate scale p is taken to be the Nyquist sampling of the telescope's diffraction limit, $\lambda/2D$. From a pointlike source of flux ϕ , the detected photon count per pixel is then assumed to be one-quarter of the flux in the central Airy core. The fractional energy in the core is reasonably well approximated by the Strehl ratio ρ , and so one obtains

$$F_{\text{target}} = \eta A \phi \rho / 4. \quad (8)$$

For a wavefront with rms phase deviation σ , the Strehl ratio is well approximated by the expression

$$\rho = e^{-\sigma^2}, \quad (9)$$

provided that $\sigma < 0.9$ rad. The results in § 5 have been derived assuming correction by the AO system to $\rho = 0.5$ in the K band, implying an rms phase deviation at that wavelength of $\sigma_K = 0.833$ rad. At other wavelengths, the Strehl ratio scales according to the expression

$$\rho(\lambda) = e^{-(\sigma_K \lambda_K / \lambda)^2}, \quad (10)$$

where $\lambda_K = 2.2 \mu\text{m}$.

4. COMPUTATION OF THE RELATIVE INTEGRATION TIME

Each of the terms in equation (1) will of course have its own associated photon noise contribution. The total noise variance v^2 in an observation of time t is simply the sum of the detected photons from all sources:

$$v^2 = t(F_{\text{thermal}} + F_{\text{sky}} + F_{\text{target}}), \quad (11)$$

where the scattered and stray light terms have been ignored. The signal for the observation is just

$$\Sigma = tF_{\text{target}}. \quad (12)$$

The comparison of the two AO systems begins by equating the respective noise-to-signal ratios and then computing the ratio of the integration times,

$$\frac{v_o}{\Sigma_o} = \frac{v_u}{\Sigma_u}, \quad (13)$$

where the subscripts o and u refer, respectively, to the thermally optimized system with the adaptive secondary and the unoptimized system with reimaging optics.

Proceeding, one finds

$$\begin{aligned} \frac{t_u}{t_o} &= \frac{F_{\text{target},o}^2 (F_{\text{thermal},u} + F_{\text{sky},u} + F_{\text{target},u})}{F_{\text{target},u}^2 (F_{\text{thermal},o} + F_{\text{sky},o} + F_{\text{target},o})} \\ &= \frac{\eta_o^2 (\epsilon_u P_\lambda + \eta_u S_\lambda)(\lambda/2D)^2 + \eta_u \phi \rho/4}{\eta_u^2 (\epsilon_o P_\lambda + \eta_o S_\lambda)(\lambda/2D)^2 + \eta_o \phi \rho/4}, \end{aligned} \quad (14)$$

where the substitution $p = \lambda/2D$ has been made, explicitly setting the plate scale to the Nyquist limit. This equation has been used to derive the results described below.

The wavelengths of interest in solving equation (14) are in the range where the thermal background makes a significant contribution and the AO is expected to provide a useful level of correction. Adaptive correction continues to be valuable out to about $15 \mu\text{m}$, beyond which the atmospheric aberration no longer limits the telescope's resolving power. At the short end of the range, thermal radiation begins to be noticeable at about $2 \mu\text{m}$. This range of wavelengths spans the standard photometric bands K , L , M , and N . The MMT's AO system will also correct to the diffraction limit in the H band, and under good seeing conditions the J band as well, but at these wavelengths $P_\lambda \ll S_\lambda$, and equation (14) reduces to

$$\frac{t_u}{t_o} = \frac{\eta_o}{\eta_u}; \quad (15)$$

that is, the advantage of the adaptive secondary system becomes solely one of throughput because of the reduced number of optical surfaces. This is also the case at all wavelengths for bright sources in which the terms in ϕ dominate.

5. RESULTS

Because of the dependence on thermal and sky background, equation (14) is a function of both the wavelength and the optical bandwidth used in the observation. Table 2 presents the characteristics of the four photometric filters for which results have been calculated (Allen 1976; McLean 1997).

The expected ratio of integration times for these four thermal filters has been calculated for the case of

TABLE 2

FILTER CHARACTERISTICS		
Band	λ (μm)	$\Delta\lambda$ (μm)
K	2.2	0.48
L	3.4	0.70
M	4.8	0.6
N	10.6	5.0

background-limited sources where $\phi \rightarrow 0$. The results are shown in Table 3 for three values of the ambient temperature which represent the mean and 10th and 90th percentiles of the distribution in Figure 2. A substantial improvement in integration time of a factor of 2–3 is made possible by the lower emissivity and higher throughput of the adaptive secondary system.

A more detailed view is presented in Figure 4, which shows the ratio as a function of the magnitude of an unresolved object in each of the four bands. As would be expected, for bright objects, the most significant source of noise is photon noise from the object itself, so the relative integration time is just the ratio of the transmittances (eq. [15]). As the source becomes fainter, the thermal term in equation (14) begins to appear, sooner for the longer wavelengths, driving the relative integration time higher. When the source brightness becomes very small compared to the

TABLE 3

RELATIVE INTEGRATION TIMES

T ($^{\circ}\text{C}$)	K	L	M	N
0.0	1.90	2.47	2.02	2.73
8.2	2.26	2.69	2.19	2.79
15.9	2.58	2.86	2.35	2.85

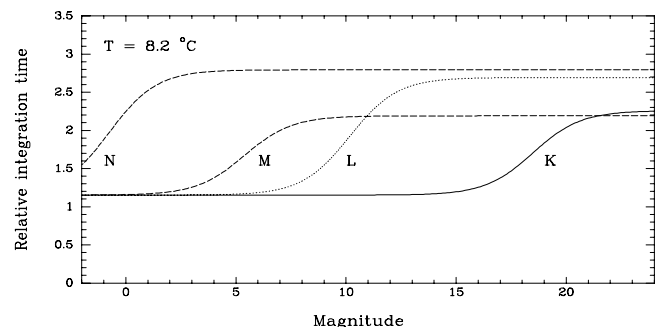


FIG. 4.—Relative integration times for unresolved sources in the four photometric bands K through N as a function of source magnitude. The ambient temperature has been taken as the mean value of Fig. 2.

combined thermal and sky background, the curves saturate at a level given by the ratio of thermal background to sky background radiation.

With $\phi = 0$, equation (14) becomes

$$\frac{t_u}{t_o} = \frac{\eta_o^2 (\epsilon_u P_\lambda + \eta_u S_\lambda)}{\eta_u^2 (\epsilon_o P_\lambda + \eta_o S_\lambda)}, \quad (16)$$

which varies between the values 1.15 for $P_\lambda \ll S_\lambda$ (eq. [15]) and 3.35 for $P_\lambda \gg S_\lambda$. The relative integration time for background-limited sources therefore grows with the ratio P_λ/S_λ . This makes intuitive sense: in regions of the spectrum where the sky is very transparent, and therefore where its emissivity is low, the effect of thermal radiation from the telescope becomes dominant, and the thermally optimized system has a stronger advantage.

Results have also been computed at all wavelengths in the range 1.8–14 μm . Figure 5 shows the relative integration time for background-limited sources observed through filters of 1%, 10%, and 20% bandwidth. The three panels correspond to ambient temperatures of 0.0°C, 8.2°C, and 15.9°C. For reference, the effective bandwidths of the four standard filters are also shown. It becomes clear from these plots that the main advantage of the adaptive secondary system is indeed, as expected, in these windows.

The PUEO design used as the basis for comparison in the results above exhibits probably the best thermal performance of any astronomical AO system in current use. Other designs, though, now being implemented on the world's large telescopes are not so well optimized in this respect; constraints imposed by budgets, volume requirements, component availability, scientific goals, and so on, have lead to a wide variety of choices. Systems for the Keck II (Wizinowich et al. 1998), Gemini North (Herriot et al. 1998), Subaru (Takami et al. 1998), and the Very Large Telescope Unit 1 (Rousset et al. 1998) telescopes, for example, all suffer from substantially higher thermal background. Table 4 summarizes their optical designs.

It is instructive to ask how well an adaptive secondary system will perform in comparison with these instruments. Results have been calculated for the cases of both the MMT and the LBT. In the case of the smaller telescope, each of the

TABLE 4

PARAMETERS OF FOUR OTHER ADAPTIVE OPTICS SYSTEMS

Telescope	m	n	D (m)
Keck II	8	6	10.0
Gemini N.....	7	6	8.1
Subaru	6	4	8.2
VLT UT1.....	7	2	8.2

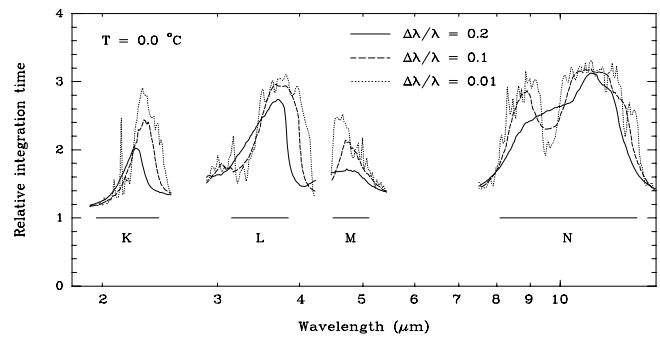


FIG. 5a

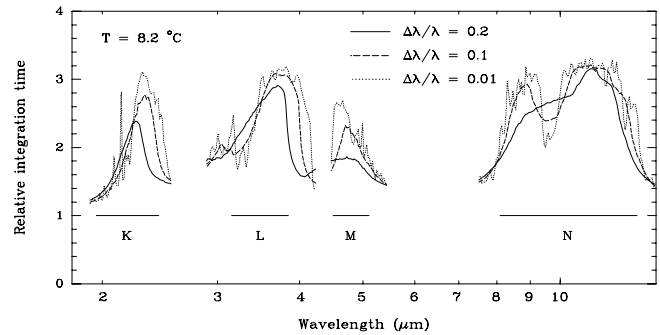


FIG. 5b

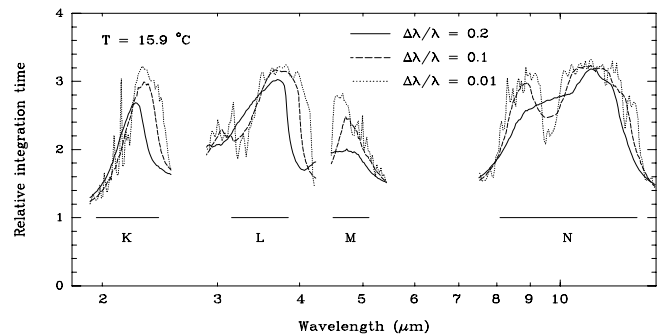


FIG. 5c

FIG. 5.—Relative integration times for the unoptimized vs. the optimized AO system as a function of wavelength. The three panels correspond to ambient temperatures of (a) 0.0°C, (b) 8.2°C, and (c) 15.9°C. Plots are shown for filters with effective bandwidths of 1%, 10%, and 20%. No data are shown where the atmospheric transmission is worse than 20%. In all cases, the pixel scale was assumed to sample the diffraction limit at the Nyquist interval of $\lambda/2D$, where λ is the central wavelength of the filter. For reference, the effective bandwidths of the four standard photometric bands K through N are also shown.

four comparison systems has a distinct advantage because of substantially greater aperture. Nonetheless, as shown in Table 5, in terms of the time required to reach a background-limited source, the lower emissivity is more important than the larger area.

A more direct comparison is possible with a single unit of the LBT in the sense that its 8.4 m diameter aperture is

TABLE 5
COMPARISON OF INTEGRATION TIMES BETWEEN THE
MMT AND OTHER LARGE TELESCOPES

Telescope	<i>K</i>	<i>L</i>	<i>M</i>	<i>N</i>
Keck II	1.72	2.18	1.65	2.28
Gemini N	2.43	3.05	2.33	3.19
Subaru	1.86	2.29	1.79	2.38
VLT UT1	1.70	2.08	1.65	2.16

closer in size to the other telescopes. Table 6 shows that in this case, the advantage offered by the adaptive secondary is even more pronounced and, in addition of course, the diffraction-limited resolution is comparable as well.

6. CONCLUSIONS

Substantial gains in near-infrared scientific throughput can be realized at a large telescope equipped with an adaptive secondary. Imaging and spectroscopy of faint sources can be accomplished not only with diffraction-limited resolution, but in perhaps one-third of the time required to do so with a conventional AO system. Indeed, when both units of the LBT are brought on line in 2004, the combination of the 23 m baseline at the interferometric focus, a collecting area of 109 m², and the low emissivity afforded by two adaptive secondaries will provide unprecedented sensitivity.

This advantage applies generally to telescopes of all sizes. If diffraction-limited pixels are used to maximize the resolution benefit provided by AO, the background limit becomes fainter as the telescope aperture increases, but once it is reached, the same gains in relative integration time shown in Table 3 will be seen. If larger pixels are used, such as might be done to obtain low- to medium-resolution spectra, the background-limited brightness will increase, and the full advantage will be seen sooner.

The biggest gains are to be made in those spectral regions where the sky is darkest, since this is where thermal emission from the optics is most important. Note that the standard broadband filters are chosen to fall into the windows of atmospheric transparency, and therefore the adaptive secondary is of most value in precisely those spectral

TABLE 6
COMPARISON OF INTEGRATION TIMES BETWEEN THE
LBT AND OTHER LARGE TELESCOPES

Telescope	<i>K</i>	<i>L</i>	<i>M</i>	<i>N</i>
Keck II	2.87	3.63	2.75	3.81
Gemini N	4.05	5.10	3.89	5.33
Subaru	3.11	3.82	2.99	3.98
VLT UT1	2.84	3.47	2.75	3.61

regions where astronomers are accustomed to observe. As a corollary, since the atmospheric background longward of 2.3 μ m is dominated by emission from water vapor, adaptive secondaries will be most important for infrared-optimized telescopes at the driest sites such as Mauna Kea.

As an example of the scientific potential, consider the work of Burrows et al. (1997) who have described detailed models of the atmospheres of substellar objects in the range (1–40) M_J (M_J = Jupiter's mass). Because of flux blanketing at longer wavelengths, these objects are expected to appear much bluer than had previously been supposed and will display flux enhancements in the 4–5 μ m range of 5 or more orders of magnitude compared to a blackbody of the same size and effective temperature. A 5 M_J planet 5 Gyr old at 10 pc has a flux at 5 μ m of about 10 mJy. Such an object would be detectable at an S/N of 6 in a 1 hr integration with the adaptive secondary system, but would require \sim 3 hr with the unoptimized system. Objects of this sort could be found in orbits down to a few AU in radius.

A practical concern in the implementation of adaptive secondaries is the need to dissipate a lot of power in the middle of the light path. The MMT secondary will need 1–2 kW, depending on the prevailing seeing. An actively controlled liquid (water/methanol) cooling system fed by pipes hidden behind the secondary spider vanes will ensure that temperature differences between the ambient air and all exposed surfaces are held to less than 1°C.

A further advantage of the adaptive secondary approach bears consideration. It has been pointed out by Racine & Ellerbroek (1995), and Herriot et al. (1998), among others, that the isoplanatic patch of an AO system can be extended by conjugating the deformable mirror to an appropriate altitude where the bulk of the turbulence is located, and further by incorporating a number of deformable mirrors, each conjugate to a separate layer of turbulence. It is observed at many telescope sites that one of the strongest turbulent layers is very close to the ground (Roddier et al. 1990; Marks et al. 1996). Therefore, in any multiconjugate AO system, one of the deformable mirrors must be placed at or near an image of this boundary layer. In the normal configurations for modern astronomical telescopes, the secondary mirror is naturally conjugated within typically a few hundred meters of the ground and is therefore ideally located to correct boundary layer turbulence. The Gregorian configuration conjugates its concave secondary at roughly 100 m above the telescope, and indeed this design will be used for the LBT. For the more usual Cassegrain design, such as the MMT, the conjugate is virtual, falling about 100 m below the ground. Nonetheless, from the optical point of view, this is still very close to the offending ground layer.

With this strong component of the aberration removed, the isoplanatic angle can more readily be expanded by the addition of a second stage of correction, using an AO

system which would resemble the conventional reimaged pupil design. If such a system can be housed in a cryogenic environment, then the advantages of high resolution, low thermal background, and a large corrected field will all be realized at once.

I am grateful to Don McCarthy and Marcia Rieke for discussions on the various terms contributing to the noise, and to George Rieke for a critical reading of the manu-

script. Many thanks to Pat Roche for the use of his sky background model, to Larry Reddell for making the WIYN reflectivity data available, and to Alejandra Milone for collecting the temperature data, which were taken at the Multiple Mirror Telescope, a joint facility of the University of Arizona and the Smithsonian Institution. This work has been supported by the Air Force Office of Scientific Research under grant F49620-94-100437.

REFERENCES

- Allen, C. W. 1976, *Astrophysical Quantities* (3d ed.; Athlone: London)
- Bawolek, E. J., Mohr, J. B., Hirleman, E. D., & Majumdar, A. 1993, *Appl. Opt.*, 32, 3377
- Burrows, A., et al. 1997, *ApJ*, 491, 856
- Fugate, R. Q., et al. 1991, *Nature* 353, 144
- Gray, P. M., West, S. C., & Gallieni, W. 1996, *Proc. SPIE*, 2871, 374
- Herriot, G., et al. 1998, *Proc. SPIE*, 3353, 488
- Hinz, P. M., et al. 1998, *Nature*, 395, 251
- Lloyd-Hart, M., et al. 1998, *Proc. SPIE*, 3353, 82
- Marks, R. D., et al. 1996, *A&AS*, 118, 385
- McLean, I. S. 1997, *Electronic Imaging in Astronomy: Detectors and Instrumentation* (Wiley: Chichester)
- Milone, A. A. E., Heller, C., & McAfee, J. 1999, MMTO Technical Memorandum 99-1
- Racine, R., & Ellerbroek, B. L. 1995, *Proc. SPIE*, 2534, 248
- Rigaut, F., et al. 1998, *PASP*, 110, 152
- Roddier, F., et al. 1990, *Proc. SPIE*, 1236, 485
- Rousset, G., et al. 1998, *Proc. SPIE*, 3353, 508
- Salinari, P., & Sandler, D. G. 1998, *Proc. SPIE*, 3353, 742
- Sandler, D. G., Stahl, S., Angel, J. R. P., Lloyd-Hart, M., & McCarthy, D. W. 1994, *J. Opt. Soc. Am. A*, 11, 925
- Takami, H., Takato, N., Otsubo, M., Kanzawa, T., Kamata, Y., Nakashima, K., & Iye, M. 1998, *Proc. SPIE*, 3353, 500
- Warner, J. W. 1977, *PASP*, 89, 724
- West, S. C., et al. 1996, *Proc. SPIE*, 2871, 38
- Wizinowich, P. L., et al. 1998, *Proc. SPIE*, 3353, 568